Fatigue Behavior of Welded Steel Butt Joints Containing Artificial Discontinuities

The effect of discontinuities on the fatigue behavior of welded steel butt joints are assessed by means of experimentation and analytical models

BY M. D. BOWMAN AND W. H. MUNSE

ABSTRACT. Zero-to-tension fatigue tests were carried out on notched low-carbon steel plain plate specimens, and on welded low-carbon steel and quenched-and-tempered steel notched specimens. Notches for the welded specimens were machined in weld metal at mid-length to simulate an internal discontinuity. A range in behavior was examined by selecting a combination of various notch types, sizes, and positions.

Analytical fatigue models were developed to estimate the fatigue behavior of notched plates. Fatigue crack initiation and propagation stages of the cyclic life were considered separately. A crack initiation model was developed using low-cycle fatigue concepts and a linear damage criterion; a crack propagation model was developed using a linear crack growth power law.

Residual stress at the notch tip, notch position, sharpness, and size were found to notably influence weldment fatigue behavior. The fatigue lives of specimens containing a notch near mid-thickness were roughly equivalent to the mean fatigue resistance of sound butt welds, while the fatigue lives of specimens containing notches near quarter-thickness were markedly lower.

Introduction

Background

The fatigue resistance of a butt weld in the as-welded condition is usually poorer than the base metal to which it is joined. The localized stress concentration resulting from the profile of the weld is responsible for this inferior fatigue resistance. However, when the toe of a weld is treated by grinding or gas tungsten arc (GTA) dressing, or when the weld reinforcement is removed entirely, then internal welding discontinuities, acting as individual stress raisers, may control the fatigue behavior.

The term "discontinuity" is used to denote an entity which interrupts the continuity of a weldment. Porosity, slag inclusions, incomplete fusion, and incomplete penetration are examples of common welding discontinuities. Usually, severe discontinuities occur as a result of improper or inadequate welding procedures. However, discontinuities can also occur inadvertently during normal welding operations. Few, if any, welds are truly free of discontinuities.

Weld quality fabrication standards should consider the degree to which weld discontinuities influence fatigue behavior. It is significant to note that fatigue cracks which emanate from internal discontinuities often develop at service loads which are well below maximum design loads. Accordingly, design standards for welded members subjected to repeated loads should be formulated by relating weldment fatigue strength levels to corresponding permissible discontinuity severities.

Purpose and Approach

The primary objective of this study was to identify and evaluate variables that influence the fatigue behavior of transverse butt welds containing internal discontinuities. The degree to which dis-

Table 1—Physical Properties of Base Metal and Weld Metal

Designation	Yield strength, ksi[a]	Tensile strength, ksi[a]	Elongation in 2 in. (50.8 mm), %	Reduction in area, %
Low-carbon steel	29.8	55.1	34.1[b]	59.1
Quenched-and-tempered steel[c]	88.5-90.0	108.3-109.2	22.6-25.3	69.2-70.4
E7018[d]	68.0	75.0	34.0	75.0
E11018[d]	103.0	115.0	22.0	62.0

(a) 1 ksi = 6.895 MPa.
(b) Percent elongation in 8 in. (203 mm).
(c) Values reported in Ref. 1 for two heats of steel.
(d) Values reported by electrode manufacturer.

Table 2—Chemical Compositions of Base Metal and Weld Metal, Wt-%

Element	Low-carbon steel	Quenched-and-tempered steel[a]	E7018[b]	E11018[b]
C	0.17	0.16-0.17	0.06	0.06
Mn	0.44	0.28-0.33	1.10	1.53
P	< 0.005	0.010-0.021	0.03	0.030
S	0.030	0.009-0.019	0.04	0.030
Si	< 0.01	0.26-0.27	0.50	0.27
Cu	0.04	0.06	–	–
Ni	< 0.01	2.29-2.86	–	1.88
Cr	0.02	1.31-1.61	–	0.31
Mo	< 0.01	0.32-0.48	0.40-0.65	0.42
Al	0.024	–	–	–

(a) Values reported in Ref. 1 for two heats of steel.
(b) Values reported by electrode manufacturer.

Paper presented at the 63rd AWS Annual Meeting held in Kansas City, Missouri, during April 25-30, 1982.

M. D. BOWMAN is Assistant Professor of Civil Engineering, Purdue University, West Lafayette, Indiana, and W. H. MUNSE is Professor Emeritus of Civil Engineering, University of Illinois at Urbana-Champaign, Urbana, Illinois.

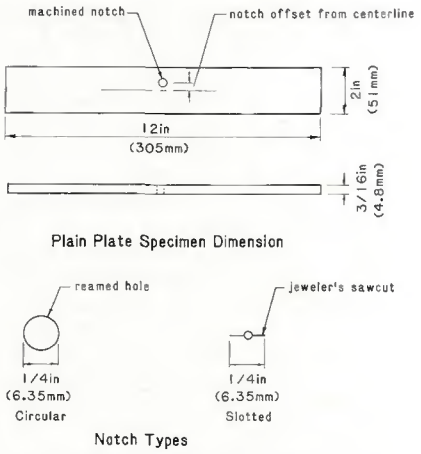

Fig. 1—Plain plate specimen dimensions and notch types

continuity size, sharpness, and position reduce the mean fatigue strength of a sound weld was examined experimentally and theoretically.

Specimens for the experimental fatigue testing program consisted of narrow plain plate and welded notched steel strips. Control of discontinuity size, shape, and position is vitally important in an evaluation of the effect of these factors. Therefore, it was decided that the best control could be obtained by using notches carefully machined in weld metal to artificially model actual discontinuities.

Analytical fatigue models for the fatigue crack initiation and propagation stages of the cyclic life were developed. The influence of residual stress on the computed fatigue lives was considered in the models for both stages of the life. Comparisons between experimental fatigue test results and predicted fatigue lives were used to evaluate the applicability and performance of the analytical fatigue models.

Experimental Test Program

Materials and Specimen Fabrication

Three different notched specimen types were tested:

1. Plain plate low-carbon steel (PP Series).
2. Welded low-carbon steel (LC Series).
3. Welded quenched-and-tempered steel (QT Series).

Table 3—Welding Procedures for Low-Carbon Steel and Quenched-and-Tempered Steel Plates

	Low-carbon steel welds	Quenched-and-tempered steel welds
Double V-groove angle, degrees	70	60
Root gap and midthickness rootface, in. (mm)	1/8 (3.2)	1/8 (3.2)
Preheat and interpass temperature, °F (°C)	None	200 (93)
Electrode type	E7018	E11018
Voltage	22-24	22-24
Root Passes:		
Number of passes	2	2
Electrode diameter, in. (mm)	5/32 (4.0)	5/32 (4.0)
Electric current, A	120-170	130-170
Average weld speed, ipm (mm/s)	5.5 (2.3)	5.0 (2.1)
Average heat input, kJ/in. (kJ/m)	38.1 (1500)	41.3 (1626)
Remaining Passes:		
Number of passes	10	10
Electrode diameter, in. (mm)	3/16 (4.8)	3/16 (4.8)
Electric current, A	230-240	220-230
Average weld speed, ipm (mm/s)	7.6 (3.2)	6.5 (2.7)
Average heat input, kJ/in. (kJ/m)	42.7 (1681)	47.9 (1886)

The PP and LC Series specimens were fabricated from a 1 in. (25 mm) thick low-carbon steel plate, while the QT Series specimens were fabricated from a 1 in. (25 mm) thick HY-80 steel plate. The shielded metal arc process was used to manually join all welded specimen plates. E7018 covered electrodes were used to weld the low-carbon steel plates, and E11018 covered electrodes were used for the quenched-and-tempered steel plates. The mechanical and chemical properties of the low-carbon steel, quenched-and-tempered steel, and the electrodes are listed in Tables 1 and 2, respectively.

Plain plate specimen blanks were removed from base metal plate such that the longitudinal axis of all specimens was parallel to the direction of plate rolling. Two test specimens were obtained from each blank by dividing the blank thickness and machining each half to a final thickness of 3/16 in. (4.76 mm). Specimens were then notched through the thickness with either a circular hole or a narrow slot.

The circular notches were formed by drilling slightly undersized holes and reaming to the desired diameter. The slots were formed by first drilling a 0.036 in. (0.89 mm) diameter hole in the plate so that a jeweler's saw blade could be inserted to cut the desired slot width. Three notch positions with respect to the width were used for each notch type: midwidth, or offset from midwidth by 0.25 in. (6.35 mm) or 0.50 in. (12.7 mm). A sketch of the specimen dimensions and notch types are shown in Fig. 1.

Twelve passes were necessary to fabricate the 12 in. (305 mm) long by 6 in. (152 mm) wide by 1 in. (25 mm) thick double plates. The underside of the root pass was backchipped and thoroughly ground before the second pass was placed. Subsequent passes were placed on opposite sides of the root to minimize distortion of the weldment. Details of the welding procedure for the low-carbon steel and the quenched-and-tempered steel welds are given in Table 3.

Welded specimens blanks were carefully removed from the 1 in. (25 mm) thick welded plates. After welding, the reinforcement was removed and the welds x-ray radiographed. In weld regions that appeared to be free of discontinuities, the plate was sectioned perpendicular to the weld axis into 1/4 in. (6.3 mm) strips, and machined to the final specimen dimensions—Fig. 2. Notches for the welded specimens were placed in weld metal using techniques similar to those used to form notches in the plain

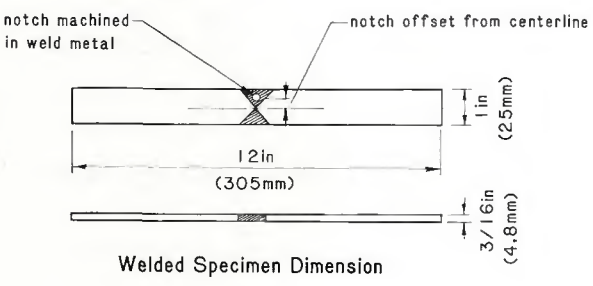

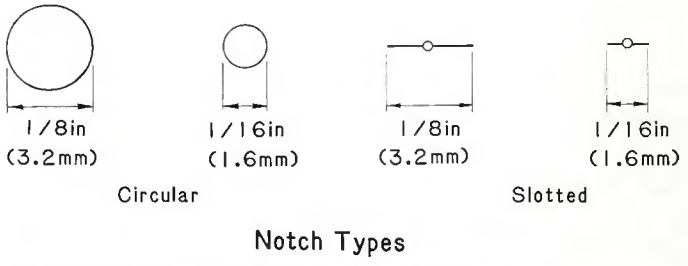

Fig. 2—Welded specimen dimensions and notch types

Table 4—Notch Details for Welded Specimens

Notch location designator	Notch offset from midwidth, in.	(mm)	Notch size[a] Hole S[b]	Hole L[b]	Slot S[b]	Slot L[b]
A	0	(0)	X	X	X	X
B	0.125	(3.2)	X	–	X	–
C	0.250	(6.3)	X	X	X	X
D	0.325	(8.3)	X	–	X	–

(a) An X-marking indicates that a specimen with given notch geometry, size, and position was fabricated and tested.
(b) S denotes 1/16 in. (1.6 mm) notch width, while L denotes 1/8 in. (3.2 mm) notch width.

plate specimens.

Table 4 indicates the two notch sizes and four notch positions through the width which were used for the welded specimens to represent a range of possible discontinuity configurations within a weldment.

Fatigue Testing

Fatigue tests were conducted under load control using a ± 50,000 lb. (222 kN) capacity closed loop, servo-hydraulic testing system. Test specimens were secured to the test frame with self-aligning hydraulic grips. All tests were performed at 68° F (20° C) under ambient laboratory conditions. The loading cycle used was zero-to-tension, applied at a frequency of 200 cpm (3.33 Hz). Loading was continued until complete specimen fracture occurred.

Two techniques were used to detect fatigue crack initiation:

1. Strain gages (Micro Measurements EA-06-062-AK-120) were mounted on the specimen surface, as closely as possible to each side of a notch, to monitor the strain range at intervals throughout a test. A notable change in the observed strain range was taken as an indication that a fatigue crack had initiated.

2. A X20 magnifying glass was used to examine the notch edges and the material at mid-thickness of a notch for evidence of crack initiation.

Cracking was first detected most reli-

Table 5—Fatigue Test Results of Notched Plain Plate Specimens

Specimen	Net stress range, ksi[a]	Initiation life, cycles	Total life, cycles	Notch offset ratio[b]	Notch type	Remarks
PP-1	30.0	45,000	88,820	0.000	Hole	
PP-2	30.0	4,000	33,350	0.000	Slot	
PP-3	30.0	64,650	136,480	0.000	Hole	Hole formed by EDM[c]
PP-4	30.0	3,000	34,540	0.003	Slot	Slot formed by EMD[c]
PP-5	30.0	60,100	134,300	0.123	Hole	
PP-6	30.0	3,000	32,360	0.130	Slot	
PP-7	30.0	55,000	102,590	0.241	Hole	
PP-8	30.0	1,000	25,850	0.256	Slot	
PP-9	25.0	514,000	943,120	0.013	Hole	Overloaded at 286,000, 730,000 and 878,400 cycles
PP-10	25.0	156,750	356,420	0.242	Hole	Precycled 1,217,000 cycles at 15.5 ksi

(a) Minimum stress was 0.5 ksi (3.5 MPa) for all tests. 1 ksi = 6.895 MPa.
(b) Ratio of notch offset from midwidth to specimen width.
(c) EDM denotes electrical discharge machining.

Table 6—Fatigue Test Results of Notched Low-Carbon Steel Welded Specimens

Specimen	Net stress range, ksi[a]	Initiation life, cycles	Total life, cycles	Notch type[b]	Notch offset ratio[c]	Location of fracture[d]	Remarks
LC-1-SAH	30.0	–	2,130,000+	H	0.002	C	Run out
LC-2-SBH	30.0	–	1,988,820+	H	0.120	E	Run out
LC-3-SCH	30.0	–	2,200,000+	H	0.258	C	Run out
LC-4-SDH	30.0	1,460,000	1,801,120	H	0.333	B	Initiation at end of slag line and pore
LC-5-LAH	30.0	932,000	1,520,420	H	0.009	A&B	Initiation at small slag line near midwidth
LC-6-LCH	26.0	647,000	1,341,350	H	0.253	A	Overloaded on 3rd cycle to +40.5 ksi
LC-7-SAS	30.0	1,896,000	4,001,870+	S	0.011	D	Run out
LC-8-SBS	30.0	–	2,190,000+	S	0.120	C	Run out
LC-9-SCS	30.0	315,000	476,010	S	0.243	A	–
LC-10-SDS	30.0	191,280	354,180	S	0.322	A	–
LC-11-LAS	30.0	568,250	2,013,000+	S	0.001	D	Run out
LC-12-LCS	30.0	31,170	91,060	S	0.247	A	–
LC-13-LCH	30.0	435,000	634,520	H	0.245	A	–

(a) Minimum stress was 0.5 ksi (3.5 MPa) for all tests. 1 ksi = 6.895 MPa.
(b) H denotes circular notch; S denotes slotted notch.
(c) Ratio of notch offset from midwidth to specimen width.
(d) The fracture mode is denoted by the following conditions: A, through the intended notch; B, through a small unintentional weld discontinuity; C, did not crack; D, cracked at notch but did not fracture; E, failed in grips, but uncracked at notch.

Table 7—Fatigue Test Results of Notched Quenched-and-Tempered Steel Welded Specimens

Specimen	Net stress range, ksi[a]	Initiation life, cycles	Total life, cycles	Notch type[b]	Notch offset ratio[c]	Location of fracture[d]	Remarks
QT-1-SAH	45.0	1,422,660	1,498,840	H	0.002	B	Initiation at small pore near plate surface
QT-2-SBH	45.0	–	2,312,850+	H	0.146	C	Run out
QT-3-SCH	45.0	996,000	1,334,070	H	0.260	A	–
QT-4-SDH	45.0	365,000	471,960	H	0.336	A	–
QT-5-LAH	45.0	–	1,306,750+	H	0.014	C	Precycled 2,110,000 cycles at 40.0 ksi (276 MPa) stress range. Run out
QT-6-LCH	40.0	265,000	361,650	H	0.268	A	Precycled 2,000,000 cycles at 26.0 ksi (179 MPa) stress range
QT-7-SAS	45.0	–	2,022,000+	S	0.003	C	Run out
QT-8-SBS	45.0	86,800	120,720	S	0.132	A	–
QT-9-SCS	45.0	30,000	106,550	S	0.253	A	–
QT-10-SDS	45.0	45,000	86,060	S	0.334	A	–
QT-11-LAS	45.0	104,250	7,066,800+	S	0.009	D	Run out
QT-12-LCS	45.0	21,000	44,070	S	0.251	A	–
QT-13-LCH	45.0	78,000	181,460	H	0.262	A	–
QT-14-LCH	36.0	894,000	1,016,990	H	0.266	B	Initiation at slag line along weld boundary

(a) Minimum stress was 0.5 ksi (3.5 MPa) for all tests. 1 ksi = 6.895 MPa.
(b) H denotes circular notch; S denotes slotted notch.
(c) Ratio of notch offset from midwidth to specimen width.
(d) The fracture mode is denoted by the following conditions: A, through the intended notch; B, through a small unintentional weld discontinuity; C, did not crack; D, cracked at notch but did not fracture.

ably using the X20 magnifying glass for specimens with circular notches, while both techniques were equally effective for specimens with slotted notches.

The propagation of surface cracks was monitored with a traveling X40 microscope. Growth of a crack on the specimen surface was determined by measuring the movement of the microscope with two 0.001 in. (0.025 mm) scale dial gages.

Fatigue Data

The results of all fatigue tests are summarized in Tables 5–7. Table 5 presents fatigue test results for the plain plate notched specimens. Tables 6 and 7 give fatigue test results for the welded low-carbon steel and quenched-and-tempered steel notched specimens, respectively. The notch type and ratio of notch offset from midwidth to specimen width are indicated also in each table.

The notched plain plate fatigue test results are compared in Fig. 3 to a mean S-N curve based upon fatigue tests conducted by Stallmeyer (Ref. 2) and Wilson, et al. (Ref. 3) on mild steel plain plate specimens containing a circular notch at midwidth. The fatigue lives for two of the three specimens with central circular notches are slightly less than one standard deviation below the mean curve, possibly indicating a somewhat lower fatigue resistance than either A7 or A36 steels.

It can be seen also that notch sharpness and offset both affect fatigue life. Specimens notched with narrow slots (small notch root radii) have shorter fatigue lives than specimens notched with circular holes of the same diameter as the slot width. Moreover, for specimens containing either of the two notch types, a reduction in fatigue life is obtained for each corresponding increase in notch offset from midwidth.

Figures 4 and 5 show the test data for the welded low-carbon steel and quenched-and-tempered steel notched specimens, respectively. Trends reflecting the effect of notch position and geometry on the fatigue behavior can be observed by comparing individual test results. Specimens containing notches near midwidth either did not crack or cracks that initiated at the notches appeared not to propagate; only three of the twelve specimens with notches at positions A or B (see Table 4) failed after 2,000,000 or more loading cycles. However, by offsetting the notch to at least quarter-thickness, positions C or D, all but one of the fifteen specimens failed.

Residual stress, in addition to notch position, undoubtedly affected the fatigue behavior of the specimens. Mean stress at the tip of notches positioned near mid-thickness is significantly reduced as a result of the compressive residual welding stress. The extent to which a reduced mean stress prolongs the fatigue

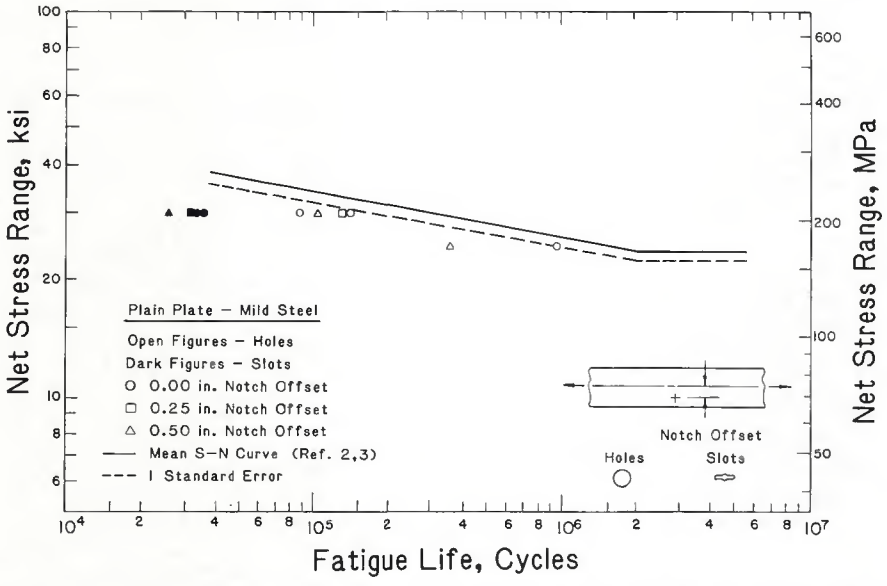

Fig. 3—Comparison of plain plate low-carbon steel notched specimen fatigue test results with a mean S-N curve for centrally notched specimens

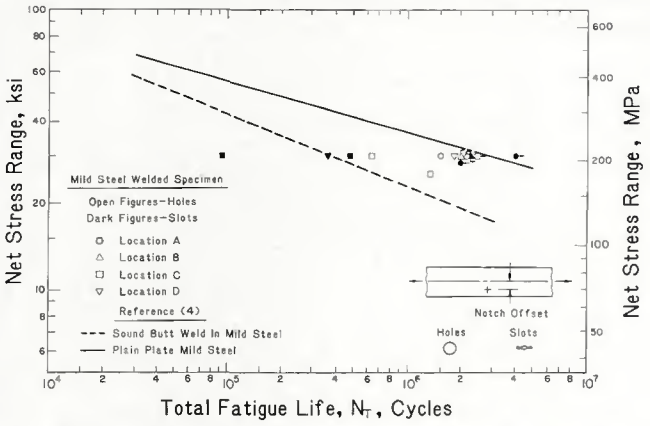

Fig. 4 – Fatigue test results for notched low-carbon steel welded specimens

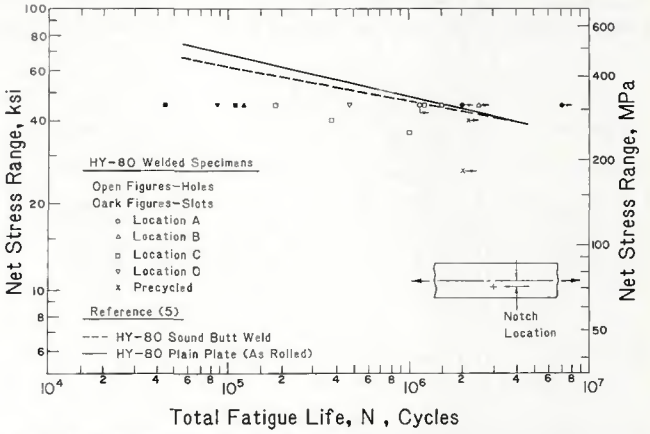

Fig. 5 – Fatigue test results for notched quenched-and-tempered steel welded specimens

life depends upon how quickly mean stresses shake down for a given material. For some materials it is possible, as Boulton (Ref. 6) reports for welds which contained slag inclusions, that the residual stress can have no effect on the fatigue strength. Moreover, work by Babaev (Ref. 7) on lack of fusion discontinuities indicates that a tensile residual stress at the notch tip can result in significant reductions in the fatigue life.

The importance of the combined effects of notch through thickness position and residual stress at the notch tip was demonstrated in the failure mode of four specimens. Small unintentional discontinuities within specimens LC-4, LC-5, QT-1, and QT-14 were severe enough stress raisers to act as preferred fatigue crack initiation sites in place of the circular through thickness notches.

Fatigue cracks initiated at small slag inclusions located close to the surface and slightly offset from midwidth for both the low-carbon steel specimens and the quenched-and-tempered steel specimens – Fig. 6. The small, unintentional discontinuities were not visible on radiographs of the welds prepared for specimen fabrication. Undoubtedly, the initiation zones were influenced by increased stresses at the discontinuities, sharp notch root radii, and an unfavorable residual stress distribution.

Fatigue Models and Data Analysis

Fatigue Crack Initiation Life

The fatigue crack initiation life N_I may be defined as the number of loading cycles necessary to initiate a macroscopic, subcritical fatigue crack. Topper, et al. (Ref. 8) defined the requirements necessary for an analysis of fatigue crack initiation life:

1. A mechanics analysis to relate nominal stresses and strains to local (notch) stresses and strains.
2. Knowledge of the cyclic stress-strain properties to determine material responses for a given stress or strain.
3. Knowledge of the fatigue properties of the metal.
4. A cumulative damage procedure which predicts N_I based on the accrued damage.

Implementation of these criteria, however, requires "a priori" identification of the critical notch location for crack initiation. Also, it has been assumed that the fatigue properties of smooth laboratory specimens can be used to represent cyclic behavior at the tip of a notch.

A modified Neuber relationship was assumed adequate for relating local and remote loadings. (Ref. 9, 10):

$$\frac{(K_f\,\Delta S)^2}{E} = \Delta\sigma \cdot \Delta\epsilon \qquad (1)$$

in which K_f is the fatigue notch factor, ΔS is the remotely applied stress range, E is Young's modulus, $\Delta\sigma$ is the notch tip stress range, and $\Delta\epsilon$ is the notch tip strain range.

Peterson's relationship (Ref. 11) was used to determine expressions for K_f as a function of the theoretical stress concentration factor K_t, a material constant A, and the notch root radius r:

$$K_f = 1 + \frac{K_t - 1}{1 + A/r} \qquad (2)$$

The value of K_t for circular and slotted notches depends upon the width of the notch perpendicular to the applied stress, the notch root radius, and a correction factor for notch position relative to the plate edge. It was assumed that the worst possible configuration for the notch root

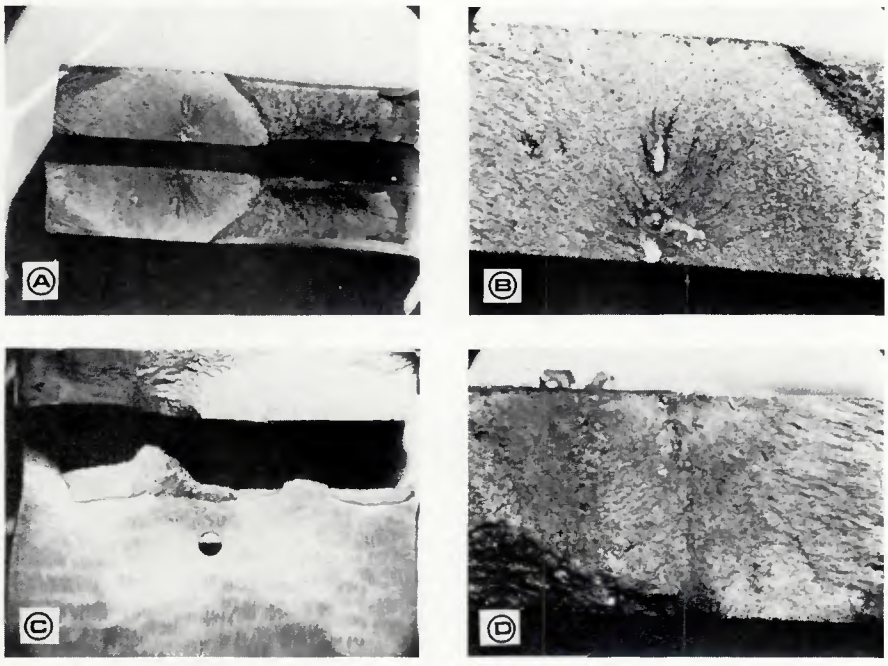

Fig. 6 – Crack initiation sites and fracture surfaces: A – LC-4 fracture surface, X3.2; B – enlargement of slag inclusion spot on fracture surface of specimen LC-4, X10; C – QT-1 fracture path, X3.2; D – enlargement of slag line on fracture surface of specimen QT-1, X10 (A, B, C, and D reduced 45% on reproduction)

radius existed at some location along the notch length. The particular notch root radius which produces the maximum fatigue notch factor $K_{f_{max}}$ can be found by solving the expression obtained by setting the derivative of the expression for K_f with respect to the root radius equal to zero.

Material constant A depends upon the ductility and ultimate tensile strength of a metal. A relationship proposed by Peterson (Ref. 12) for heat treated steels was utilized:

$$A = \begin{matrix} 0.001(300/S_U)^{1.8} \text{ (in.)} \\ \text{-or-} \\ 0.0254(2070/S_U)^{1.8} \text{ (mm)} \end{matrix} \quad (3)$$

where S_U is the ultimate tensile strength in ksi (MPa).

A curve for the cyclic stress-strain behavior of a metal can be obtained by connecting the tips of stable hysteresis loops for companion specimens tested at different strain amplitudes. The total strain amplitude is composed of elastic and plastic portions, and may be described by (Ref. 13):

$$\frac{\Delta\epsilon}{2} = \frac{\Delta\sigma}{2E} + \left[\frac{\Delta\sigma}{2K'}\right]^{\frac{1}{n'}} \quad (4)$$

in which K′ is the cyclic strength coefficient, and n′ is the cyclic strain hardening exponent.

The total notch root strain amplitude, elastic plus plastic, and the fatigue crack initiation life for a smooth specimen $2N_f$ are given in Morrow's (Ref. 14) equation as:

$$\frac{\Delta\epsilon}{2} = \frac{\sigma'_f}{E}(2N_f)^b + \epsilon'_f(2N_f)^c \quad (5)$$

in which σ'_f is the fatigue strength coefficient, b is the fatigue strength exponent, ϵ'_f is the fatigue ductility coefficient, and c is the fatigue ductility exponent.

The fatigue damage for a particular loading reversal may be defined as the inverse of the fatigue life; here the fatigue life represents the life required for failure of a smooth specimen subjected to a constant strain amplitude equivalent to the strain amplitude applied during the loading reversal. The damage caused by each loading reversal is accumulated until a limiting damage criterion is satisfied. Using Miner's (Ref. 15) linear cumulative damage rule, the number of loading cycles required for fatigue crack initiation can be obtained by summing individual damage components on a reversal-by-reversal basis until the accrued damage equals unity:

$$\sum_{i=1}^{2N_I} \left(\frac{1}{2N_f}\right)_i = 1.0 \quad (6)$$

The four basic requirements must be combined to determine the fatigue crack initiation life. For each reversal, the remote loading range is input to the mechanics analysis, equation (1), and combined with the cyclic stress-strain curve, equation (4), to determine values of the local stress and strain ranges. The fatigue life relation, equation (5), and the local strain amplitude are then combined to determine the damage for the reversal, and added to the accumulated damage. Fatigue crack initiation is assumed to have occurred when the damage criterion is satisfied.

A computer program was developed to compute the fatigue crack initiation life. The local stresses and strains for each reversal are determined according to Neuber control, using the computer to trace the cyclic hysteresis loop.

Fatigue Crack Propagation

The fatigue crack propagation life N_p is the number of loading cycles necessary to propagate a crack from a macroscopic, subcritical size to a critical size associated with failure. The crack propagation behavior of weld metal (Ref. 16-18), and the propagation of cracks from specific types of weld discontinuities (Ref. 18-23) have been studied extensively. Typically, crack propagation lives are computed based on the power law relationship for fatigue crack growth (Ref. 24):

$$da/dN = C(\Delta K)^m \quad (7)$$

in which C and m are material constants, and ΔK is the stress-intensity factor range. The form of the stress-intensity factor may be expressed as (Ref. 25):

$$\Delta K = \Delta S \sqrt{\pi a}\, F_E\, F_S\, F_W\, F_G \quad (8)$$

in which ΔS is the remotely applied stress range, a is the half-width of the crack, and F_E, F_S, F_W, and F_G are crack size correction factors that account for the effects of an elliptical crack front, free surface, finite plate width, and nonuniform opening stresses, respectively.

The fatigue crack propagation life can be computed by transposing the variables of equation (7), and integrating over the entire crack width:

$$N_P = \int_{N_I}^{N_T} dN = \int_{a_i}^{a_f} \frac{da}{C(\Delta K)^m} \quad (9)$$

in which a_i and a_f are the initial and final half crack widths. However, the stress-intensity factor is seldom a simple expression and a closed form solution of equation (9) is often impractical. Consequently, numerical integration was used to estimate the propagation life. The crack width was divided into increments, Δa, small enough to minimize errors in the iteration procedure. Increments of the propagation life were then summed over the entire crack width:

$$N_P = \sum_{a_i}^{a_f} \frac{\Delta a}{C(\Delta K_{avg})^m} \quad (10)$$

in which ΔK_{avg} is the stress-intensity range evaluated at the average half crack width a_{avg} for a given interval.

Data Analysis

Comparisons between the computed and observed fatigue crack initiation and propagation lives are shown in Fig. 7 for the plain plate notched specimens. Estimates of the fatigue crack initiation lives for the test specimens were computed

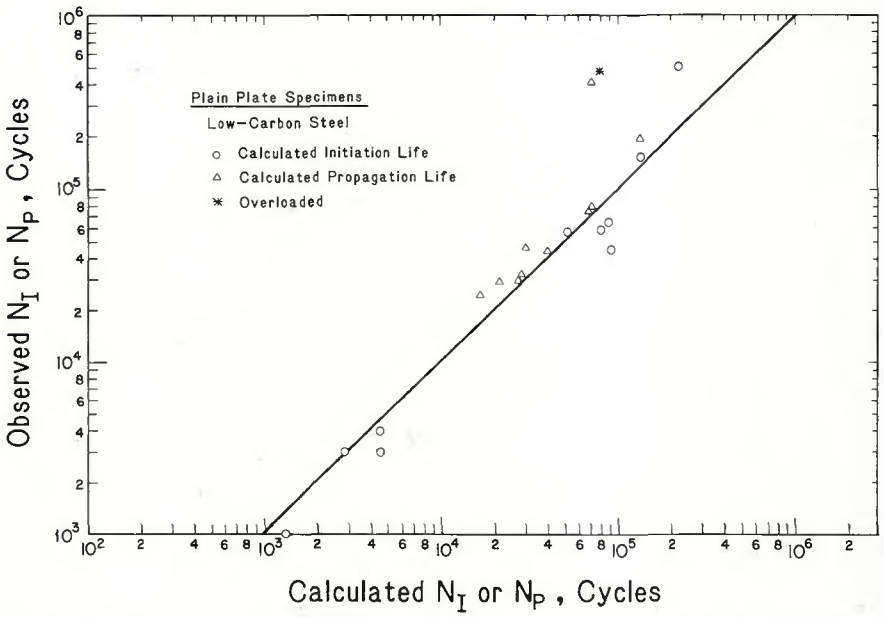

Fig. 7 — Comparison of computed and observed fatigue crack initiation and propagation lives for low-carbon steel plain plate specimens

Table 8—Low Cycle Fatigue and Cyclic Properties

	A 36[a]	E60[b]	E110[b]
K′, ksi[c]	158.75	179.0	242.0
n′	0.249	0.197	0.166
E, ksi[c]	27,500	27,400	30,300
σ'_f, ksi[c]	147.4	149.0	204.0
b	−0.132	−0.090	−0.079
ϵ'_f	0.271	0.602	0.595
c	−0.451	−0.567	−0.590

(a) Data from Mattos (Ref. 26).
(b) Data from Higashida (Ref. 27).
(c) 1 ksi = 6.895 MPa.

using the cyclic properties of A-36 base metal—Table 8 (Ref. 26). Reasonably good comparisons were obtained between the computed and observed fatigue crack initiation lives.

The fatigue crack propagation lives for the plain plate specimens were computed in two stages:

1. The life necessary to propagate a small elliptical crack through the thickness of the specimen.
2. The life required to propagate a through thickness crack to failure.

The material constants which describe the crack growth rate were determined from a least-squares fit of crack growth data taken for the five center notched specimens—Fig. 8. The computed crack propagation lives were obtained by iterating over the crack width from an assumed initial crack size of 0.01 in. (0.25 mm). The computed crack propagation lives compare very favorably with the observed crack propagation lives, with the exception of one specimen which experienced an accidental tensile overload.

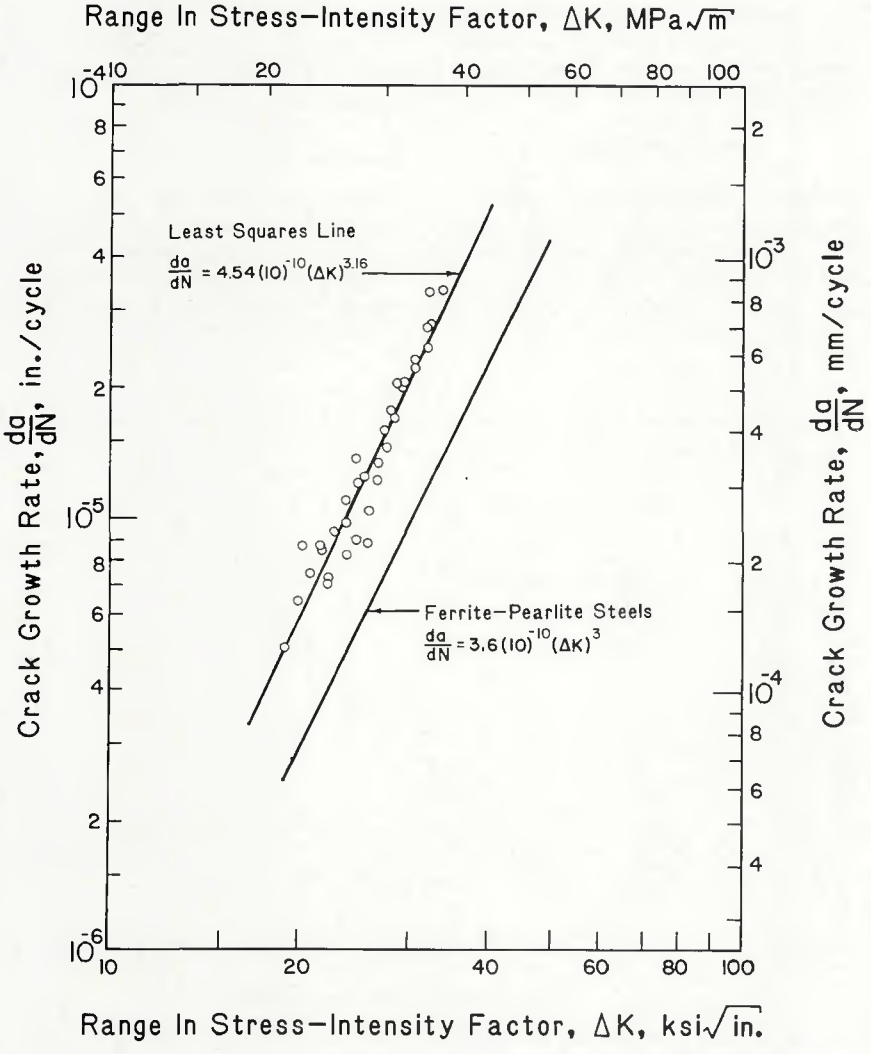

Fig. 8—Fatigue crack growth data for centrally notched low-carbon steel plain plate specimens

Comparisons between observed and computed fatigue crack initiation lives for the notched, welded specimens are shown in Fig. 9. Notable scatter of the data about the line of perfect comparison suggests that uncertainty of the residual stress at the notch root of the specimen had an affect on the computed initiation lives, especially when considering the success in modeling the initiation lives of plain plate specimens with similar geometries. Note that in most cases the computed initiation lives are less than the observed initiation lives. The conservative nature of the initiation model and the possibility that cracks initiated before they were detected could be responsible for this result.

Estimates of the fatigue crack initiation lives for the notched, welded specimens were computed using the cyclic and fatigue properties of either E60 or E110 weld metal listed in Table 8 (Ref. 27) and an assumed residual stress S_r, consistent with notch position. Residual stress for the initiation fatigue model was induced at the notch root by application of an initial setup loading cycle that resulted in the desired stress level.

A compressive residual stress of yield-point magnitude of the base metal ($S_r = -S_{YBM}$) was assumed to exist at the tip of notches near mid-thickness (positions A, B, and C); while zero residual stress ($S_r = O$) was assumed to exist at the tip of notches near quarter-thickness (positions C and D). Both residual stress states, as indicated in Fig. 9, were utilized in computing the initiation lives for specimens with notches in position C since the residual stress transition zone can be quite variable. Tensile residual stresses were not considered, since no notches were positioned adjacent to the plate surface.

Comparisons between observed and computed fatigue crack propagation lives for the notched, welded specimens are shown in Fig. 10. A small, but reasonable, crack size that would exist at an early stage in the fatigue life was selected for computing the crack propagation life. An initial crack size of 0.01 in. (0.25 mm) was selected for low-carbon welded specimens, while an initial crack size of 0.005 in. (0.12 mm) was selected for quenched-and-tempered welded specimens.

Crack propagation fatigue lives for all specimens were computed for a range in behavior corresponding either to crack growth in base metal ($S_r = O$) or to slower crack growth in weld metal as a result of compressive residual stresses ($S_r = -S_{YBM}$). Table 9 summarizes crack growth rate constants for the base metals and E70 and E110 weld metals (Ref. 17,18,28). The computed crack propagation lives bound the observed behavior, indicating that the actual crack growth rate is in between the two assumed limits. This result reinforces the assumption that

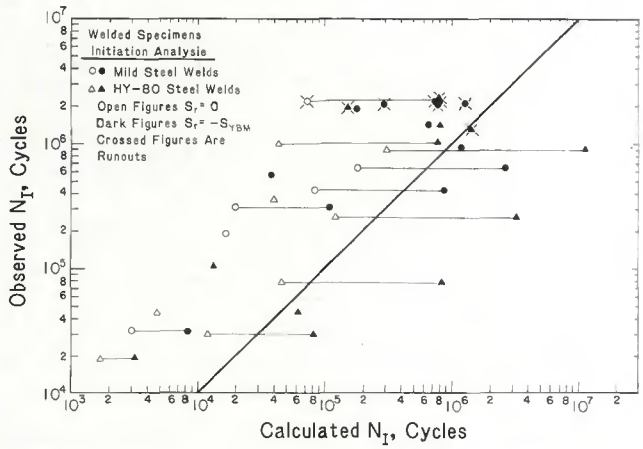

Fig. 9 — Comparison of computed and observed fatigue crack initiation lives for notched welded specimens

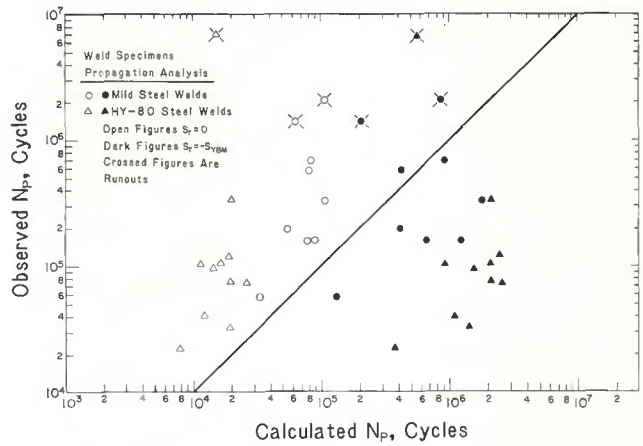

Fig. 10 — Comparison of computed and observed fatigue crack propagation lives for notched welded specimens

Table 9—Crack Growth Parameters

Material	m	C, ksi in.$^{1/2}$[d]
Ferrite pearlite steel average[a]	3.0	$3.6(10)^{-10}$
Martensitic steel average[a]	2.25	$6.6(10)^{-9}$
E70[b]	5.8	$2.7(10)^{-14}$
E110[c]	2.4	$3.2(10)^{-9}$

(a) Data from Barsom (Ref. 28).
(b) Data from Lawrence et al. (Ref. 18).
(c) Based on plot of data by Parry et al. (Ref. 17).
(d) 1 ksi in.$^{1/2}$ = 1.0986 MN m$^{-3/2}$

compressive residual stresses influence the growth of cracks positioned near the middle of welds.

Conclusion

The effect that discontinuities have on the fatigue resistance of a steel butt weldment depends upon the stress range, mean stress (as affected by residual stresses), material strength, and discontinuity shape, size, and position. Experimental results of this study indicate that notch through thickness position and sharpness at the tip of a notch can be just as critical as discontinuity size. This result was exemplified by the fatigue behavior of four test specimens which contained small, sharp unintentional slag inclusions that acted as preferred points of fatigue crack initiation in lieu of larger machined notches located near mid-thickness.

Residual stress distribution through the thickness plays an influential role in fatigue crack initiation and propagation of welded members. The majority of specimens with notches located near mid-thickness, in a beneficial compressive residual stress zone, had fatigue lives equivalent to or greater than the fatigue resistance of a sound butt weldment. Conversely, specimens with notches located near quarter-thickness, in a zone of low compressive or tensile residual stress, had markedly lower fatigue lives.

Analytical models have been developed to estimate the fatigue crack initiation and propagation portions of the total cyclic life of butt welded members containing a well defined discontinuity. Consideration of the effects of material strength and notch position, shape, and size resulted in favorable comparisons between computed fatigue lives and the notched plain plate test data. However, consideration of the effects of weld strength, notch details, and an assumed range of values for notch root residual stress resulted in computed fatigue lives bounding the welded specimen test data. Reliable estimates of the computed fatigue behavior of butt weldments can only be obtained by precisely defining the notch size, sharpness, position, and associated notch root residual stresses.

Acknowledgments

The authors wish to acknowledge that the experimental data and theoretical studies discussed herein were part of an investigation sponsored at the University of Illinois by the Illinois Division of Highways, the U.S. Department of Transportation, Federal Highway Administration, and the U.S. Navy, David W. Taylor Naval Ship Research and Development Center.

The opinions expressed herein are those of the authors and not necessarily those of the supporting agencies.

References

1. Munse, W.H., Bruckner, W.H., Hartmann, A.J., Radziminski, J.B., Hinton, R.W., and Mooney, J.L. 1964. *Studies of the fatigue behavior of butt-welded joints in HY-80 and HY-100 steels.* Structural Research Series, no. 285. Urbana, IL: University of Illinois.

2. Stallmeyer, J.E. 1953. *The effect of stress history on cumulative damage in fatigue.* Ph.D. dissertation. Urbana, IL: University of Illinois.

3. Wilson, W.M., and Thomas, F.P. 1938. *Fatigue tests of riveted joints.* Engineering Experiment Station Bulletin, no. 302. Urbana, IL: University of Illinois.

4. Radziminski, J.B., Srinivasan, R., Moore, D., Thrasher, C., and Munse, W.H. 1973. *Fatigue data bank and data analysis investigation.* Structural Research Series, no. 405. Urbana, IL: University of Illinois.

5. Hartmann, A.J., and Munse, W.H., 1962. *Fatigue behavior of welded joints and weldments in HY-80 steel subjected to axial loadings.* Structural Research Series, no. 250. Urbana, IL: University of Illinois.

6. Boulton, C.F. 1976. The influence of residual stress on the fatigue strength of butt welded joints containing slag defects. *The Welding Inst.*

7. Babaev, A.V. 1978. Examination of the effect of lack of penetration defects on the endurance of welded joints taking residual stresses into account. *Avt. Svarka (Auto. Weld.)* 31(6).

8. Topper, T.H., and Morrow, J. 1970. *Simulation of the fatigue behavior at the notch root in spectrum loaded members.* Theoretical and Applied Mechanics Report, no. 333. Urbana, IL: University of Illinois.

9. Neuber, H. 1961. Theory of stress concentration for shear strained prismatical bodies with arbitrary nonlinear stress-strain laws. *J. Appl. Mech.* Trans. Am. Soc. Mech. Engrs. series E. 28(4): 544-550.

10. Topper, T.H., Wetzel, R.M., and Morrow, J. 1969. Neuber's rule applied to fatigue of notched specimens. *J. Mater.* 4(1): 200-209.

11. Petersen, R.E. 1963. Fatigue of metals — engineering and design aspects. *Mater. Res. Std.* 3(2): 122-139.

12. Petersen, R.E., 1959. Notch sensitivity (chap. 13). *Metal fatigue.* eds. G. Sines and J.L. Waisman. New York: McGraw-Hill.

13. Morrow, J. 1965. Cyclic plastic strain energy and fatigue of metals. In *Internal fric-*

tion, damping, and cyclic plasticity. Spec. Tech. Publ. 378, pp. 45-84. Philadephia: Am. Soc. Testing Mater.

14. Morrow, J. 1968. *SAE fatigue design handbook:* 21-30 (sect. 3.2). New York: Society of Automative Engineers.

15. Miner, M. 1945. Cumulative damage in fatigue. *J. Appl. Mech.* Trans. Am. Soc. Mech. Engrs. 12(3): A159 to A164.

16. Maddox, S.J. 1974. Fatigue crack propagation data obtained from parent plate, weld metal and haz in structural steels. *Welding Research International* 4(1).

17. Parry, M., Noordberg, H., and Hertzberg, R.W. 1972. Fatigue crack propagation in A514 base plate and welded joints. *Welding Journal* 51(10): 485-s to 490-s.

18. Lawrence, F.V., Jr., and Munse, W.H. 1973. Fatigue crack propagation in butt welds containing joint penetration defects. *Welding Journal* 52(5): 221-s to 225-s.

19. Tobe, Y., and Lawrence, F.V., Jr. 1977. Effect of inadequate joint penetration on fatigue resistance of high strength structural steel welds. *Welding Journal* 55(9): 259-s to 266-s.

20. Boulton, C.F. 1976. Fatigue life predictions of welded specimens containing lack of penetration defects at ambient and elevated temperatures. *Pressure Vessels and Piping* 4(3).

21. Clark, W.G., Jr. 1973 (Sept.). The effect of hydrogen gas on the fatigue crack growth rate behavior of HY-80 and HY-130 steels. Proceedings of international conf. on the effects of hydrogen gas on material properties.

22. Fujii, E., Hayashi, S., and Iida, K. 1975. Fatigue crack propagation from a weld defect in 100 mm thick joint. *Journal of the Japanese Welding Soc.* 44(8).

23. Yamada, K., and Hirt, M.A. 1982. Fatigue crack propagation from fillet weld toes. *J. Struct. Div.* Am. Soc. Civil Engrs. 108(7): 1526-1540.

24. Paris, P., and Erdogan, F. 1963. A critical analysis of crack propagation laws. *J. Basic Eng.* Trans. Am. Soc. Mech. Engrs. series D. 85(4): 528-534.

25. Albrecht, P., and Yamada, K. 1977. Rapid calculation of stress intensity factors. *J. Struct. Div.* Am. Soc. Civil Engrs. 103(2): 377-389.

26. Mattos, R.J. 1975. *Estimation of the fatigue crack initiation life in welds using low cycle fatigue concepts.* Ph.D. dissertation. Urbana, IL: University of Illinois.

27. Higashida, Y. 1976. *Strain controlled fatigue behavior of weld metal and heat-affected base metal in A36 and A514 steel welds.* Ph.D. dissertation. Urbana, IL: University of Illinois.

28. Barsom, J.M. 1971 (May). Fatigue-crack propagation in steels of various yield strengths. Paper presented at First National Congress on Pressure Vessels and Piping at San Francisco.

WRC Bulletin 281
October, 1982

Hydrodynamic Response of Fluid Coupled Cylinders, Simplified Damping and Inertia Coefficients
by S. J. Brown

This study presents the development of the concept of inertia and damping coefficients in an historical context with experimental, classical and numerical investigations into the dynamics of fluid coupled cylinders. It is shown that coefficients may be used to account for coaxial cylinder end conditions, eccentricity, skewness, clusters, shell modes and axial modes.

Publication of this report was sponsored by the Subcommittee on Dynamic Analysis of Pressure Components of the Pressure Vessel Research Committee of the Welding Research Council.

The price of WRC Bulletin 281 is $11.50 per copy, plus $3.00 for postage and handling (foreign + $5.00). Orders should be sent with payment to the Welding Research Council, 345 E. 47th St., Room 1301, New York, NY 10017.

WRC Bulletin 282
November, 1982

Elastic-Plastic Buckling of Axially Compressed Ring Stiffened Cylinders—Test vs. Theory
by D. Bushnell

Concern for the safety of nuclear plants and offshore structures has stimulated efforts to determine buckling characteristics of stiffened cylindrical steel shells.

In this paper, BOSOR 5 computer programs were used to predict buckling loads of forty axially compressed mild steel cylindrical shells previously tested at Chicago Bridge & Iron Co.

Publication of this report was sponsored by the Subcommittee on Shells of the Pressure Vessel Research Committee of the Welding Research Council.

The price of WRC Bulletin 282 is $10.75 per copy plus $3.00 for postage and handling (foreign + $5.00). Orders should be sent with payment to the Welding Research Council, 345 E. 47th St., Room 1301, New York, NY 10017.